

Lauer, Kevin; Peh, Katharina; Krischok, Stefan; Reiß, Stephanie; Hiller, Erik; Ortlepp, Thomas

Development of low-gain avalanche detectors in the frame of the acceptor removal phenomenon

Original published in: Physica status solidi. A. - Weinheim : Wiley-VCH. - 219 (2022), 17, art. 2200177, 7 pp.
Original published: 2022-05-19
ISSN: 1521-396X ; 1862-6319 ; |p|0031-8965
DOI: [10.1002/pssa.202200177](https://doi.org/10.1002/pssa.202200177)
[Visited: 2022-10-12]



This work is licensed under a [Creative Commons Attribution 4.0 International license](https://creativecommons.org/licenses/by/4.0/). To view a copy of this license, visit <https://creativecommons.org/licenses/by/4.0/>

Development of Low-Gain Avalanche Detectors in the Frame of the Acceptor Removal Phenomenon

Kevin Lauer,* Katharina Peh, Stefan Krischok, Stephanie Reiß, Erik Hiller, and Thomas Ortlepp


Low-gain avalanche detectors (LGAD) suffer from an acceptor removal phenomenon due to irradiation. This acceptor removal phenomenon is investigated in boron, gallium, and indium implanted samples by 4-point-probe (4pp) measurements, low-temperature photoluminescence spectroscopy (LTPL), and secondary ion mass spectrometry (SIMS) before and after irradiation with electrons and protons. Different co-implantation species are evaluated with respect to their ability to reduce the acceptor removal phenomenon. In case of boron, the beneficial effect is found to be most pronounced for the low-dose fluorine and high-dose nitrogen co-implantation. In case of gallium, the low-dose implantations of carbon and oxygen are found to be beneficial. For indium, the different co-implantation species have no beneficial effect. SIMS boron concentration depth profiles measured before and after irradiation show no indication of a fast movement of boron at room temperature. Hence, the discussed $B_{Si}-Si_i$ -defect explanation approach of the acceptor removal phenomenon seems to be more likely than the other discussed B_i-O_i -defect explanation approach.

1. Introduction

Fast silicon detectors are crucial for a lot of applications,^[1] e.g., the experiments at large hadron collider (LHC) at CERN to obtain time-resolved trajectories of particles. A concept to realize such fast silicon detectors are the low-gain avalanche detectors (LGAD). They combine the advantages of normal n-i-p-diodes such as a low noise with a large signal of avalanche multiplication diodes.^[2] LGADs operate with a gain of about 10. The avalanche multiplication region is usually obtained by deep boron doped layers.^[3] Nevertheless,

K. Lauer, S. Reiß, E. Hiller, T. Ortlepp
CiS Forschungsinstitut für Mikrosensorik GmbH
Konrad-Zuse-Str. 14, 99099 Erfurt, Germany
E-mail: kevin.lauer@tu-ilmenau.de

K. Lauer, K. Peh, S. Krischok
TU Ilmenau
Institut für Physik und Institut für Mikro- und Nanotechnologien
98693 Ilmenau, Germany

 The ORCID identification number(s) for the author(s) of this article can be found under <https://doi.org/10.1002/pssa.202200177>.

© 2022 The Authors. physica status solidi (a) applications and materials science published by Wiley-VCH GmbH. This is an open access article under the terms of the Creative Commons Attribution License, which permits use, distribution and reproduction in any medium, provided the original work is properly cited.

DOI: 10.1002/pssa.202200177

these LGADs have a drawback if they are irradiated. The gain layer “disappears” after irradiation as a consequence of a deactivation of the gain layer doping species, which is usually boron.^[4,5] This means that, e.g., boron, loses after irradiation its properties as an acceptor to provide a negative space charge.

In this contribution, the focus is first on LGAD device manufacturing at CiS. Afterward, an experiment is described and discussed, which investigates the acceptor removal phenomenon for the three acceptors boron, gallium, and indium in silicon. Therefore, boron, gallium, and indium were implanted into silicon. Additionally, co-implantation of carbon, oxygen, nitrogen, and fluorine was made. It was found in the literature that for carbon co-implantation the acceptor removal effect can be reduced.^[6] Therefore, this study investigates different co-implantation species if they have an impact on the acceptor removal phenomenon.

The samples underwent an activation anneal and were then investigated by 4-point-probe (4pp), low temperature photoluminescence spectroscopy (LTPL) and secondary ion mass spectrometry (SIMS) before and after irradiation with electrons and protons.

2. Development of LGADs

The LGAD concept was realized at the CiS research institute. Two types of wafers were used to produce LGADs. These are p-type FZ silicon wafers with a resistivity larger than 10 kΩcm and silicon wafers with a 50 μm p-type epitaxial layer with a resistivity larger than 3 kΩcm. First, the conditions for the implantation and annealing of the phosphorous-doped emitter layer and the boron-doped gain layer were simulated by ATLAS software from Silvaco. From these simulations, the gain was calculated to find the proper LGAD production and working conditions.

The dopant concentration depth profiles of the phosphorous-doped emitter and the boron-doped gain-layer are depicted in **Figure 1**. Additionally, the simulated phosphorous and boron profiles are plotted as well. A good congruence between the simulation and the SIMS depth profiles is found, which shows that the simulation parameters are appropriate.

The gain as a function of the reverse voltage of one produced LGAD is shown in **Figure 2** before and after proton irradiation. The gain is obtained from the quotient of the current measured on a device with gain layer and on a device without gain layer.

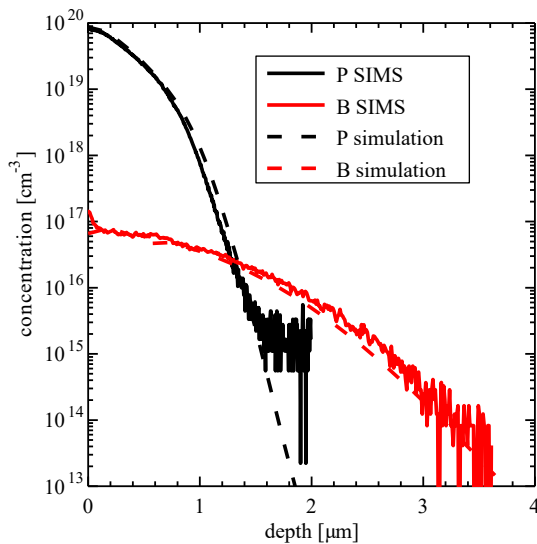


Figure 1. Dopant concentration depth profiles of phosphorous and boron of an $n^{++}-p^{+}$ -Low-gain avalanche detectors (LGAD) emitter and gain layer region obtained by secondary ion mass spectrometry (SIMS). Simulations of the phosphorous and boron profiles are plotted as well.

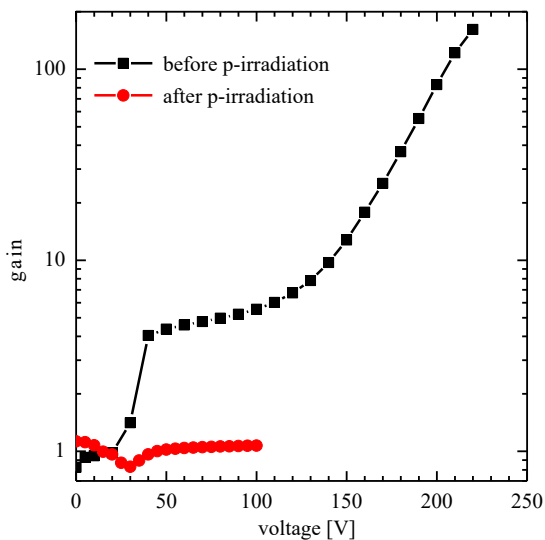


Figure 2. Gain of a produced LGAD as a function of the reverse bias voltage before and after proton irradiation.

A green laser was used as steady state excitation source. The LGADs start to amplify the current when the gain layer is fully depleted which is achieved in this case at about 40 V. This gain is found to disappear under irradiation^[4] which is related to an acceptor removal phenomenon.^[5,7]

3. Experimental Section

To investigate the acceptor removal phenomenon in LGADs, three different acceptors, boron, gallium, and indium, were implanted into high resistivity (>10 k Ω cm) boron-doped $\langle 111 \rangle$ FZ silicon wafers (s. Table 1) for this study.

Table 1. Implantation-dose and -energy for the different acceptors.

Dopant	Dose [cm^{-2}]	Energy [keV]
Boron	4.9×10^{12}	102
Gallium	4.6×10^{12}	138
Indium	3.1×10^{13}	152

Table 2. Implantation-dose and -energy for the different co-implanted species.

Dopant	Low dose [cm^{-2}]	High dose [cm^{-2}]	Energy [keV]
Carbon	2.3×10^{13}	2.4×10^{14}	110
Nitrogen	4.6×10^{12}	4.6×10^{13}	110
Oxygen	4.8×10^{12}	4.9×10^{13}	110
Fluorine	4.8×10^{12}	4.9×10^{13}	110

Additionally, oxygen, nitrogen, carbon, and fluorine were co-implanted (s. Table 2) with a low dose for each acceptor. The acceptors, boron and indium, additionally received a high dose co-implantation. Before implantation, a 100 nm thermal oxide was grown on both sides of the wafers. Overall, 25 wafers were processed. After implantation, a rapid thermal process (RTP) for 10 s at 1000 °C was applied to activate the acceptors. After RTP, the 100 nm thermal oxide was etched off. Each wafer was broken into pieces and two of the pieces per wafer were irradiated: One piece per wafer with 1 MeV electrons (dose of $4 \times 10^{11} \text{ n}_{\text{eq}} \text{ cm}^{-2}$) and the other one with 23 MeV protons (dose of $10^{15} \text{ n}_{\text{eq}} \text{ cm}^{-2}$). The electron irradiation was chosen to have point defects prevailing as radiation damage, whereas the proton irradiation was chosen to have larger defect clusters prevailing. The samples were irradiated at about room temperature. Afterward, the samples were investigated by 4pp, LTPL spectroscopy and SIMS.

Using 4pp the sheet resistance of three pieces for each wafer (implanted, electron- and proton-irradiated) was obtained.^[8] The sheet resistance was measured at five points. From these five measurements, the highest and lowest value were discarded and from the remaining three values the average and the deviation of the sheet resistance were calculated. The results are shown in Figure 3. The deviation between the three measurements is plotted as error bar, respectively.

The LTPL setup consists of a frequency doubled Nd:YAG Laser, a He flow cryostat, an imaging monochromator with 750 mm focal length and three ruled gratings with 150, 600 and 1200 grooves mm^{-1} and an InGaAs line array detector. Photoluminescence (PL) spectra are taken using a laser power of 100 mW and a beam diameter of 2 mm. The spectra are measured while storing the samples in a bath of liquid helium. Samples were broken from each piece per wafer with a size of approximately $10 \times 10 \text{ mm}^2$. The results of the LTPL measurements on the samples are shown in Figures 4 and 5.

The SIMS tool used for this study is a CAMECA IMS 7f auto at CiS Analytic Competence Center (CAK). It is a dynamic SIMS^[8] with double focusing secondary beam and two species, namely oxygen and cesium, for the primary beam. The oxygen ion source was used for the analysis of boron and the cesium source for

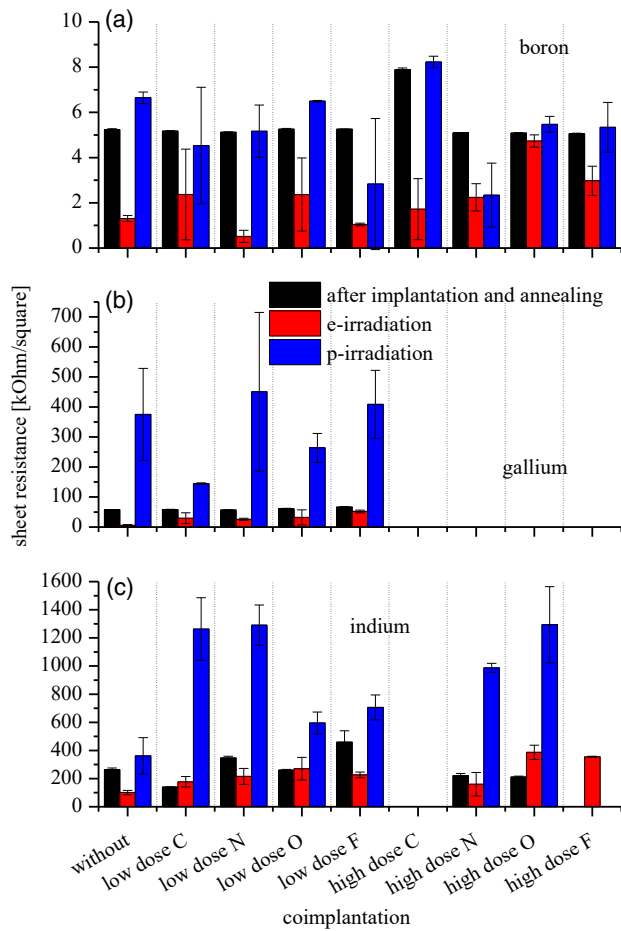


Figure 3. Sheet resistance of the samples as a function of the co-implantation type for the acceptors a) boron, b) gallium, and c) indium.

analyzing phosphor (Figure 1). Particles caused by the breaking of wafers sticking onto the samples were softly removed prior to the SIMS analysis to avoid any falsification of the measured depth profiles. Ion imaging performed via a channel plate during the SIMS measurements proved a homogenous lateral silicon and boron/phosphorous distribution and hence, the absence of disturbing particulates. The boron depth profiles shown in Figures 6 and 7 are obtained by using positive oxygen primary ions (primary high voltage 15 kV, beam diameter 11 μm , primary current 70 nA) and analyzing the positive secondary ions $^{11}\text{B}^+$ and $^{28}\text{Si}^+$.

4. Results and Discussion

The sheet resistance measured as described earlier is plotted for all samples in Figure 3. It is shown as a function of the different co-implantations. The sheet resistance measured prior to irradiation is compared to the sheet resistance measured after electron and proton irradiation.

In the unirradiated cases, the impact of the co-implantation on the activation of the dopants can be observed. In case of boron and gallium the sheet resistance is quite constant for the

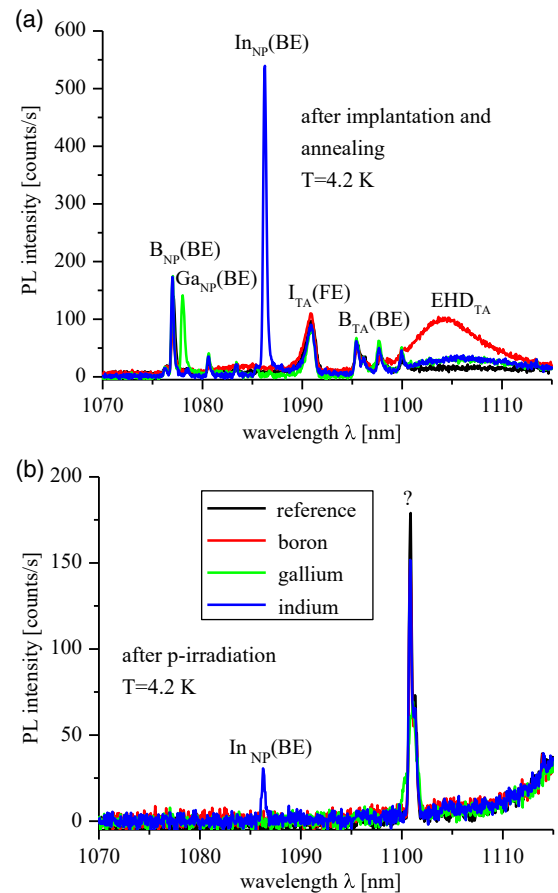


Figure 4. Low-temperature photoluminescence spectroscopy (LTPL) spectra of boron, gallium, and indium implanted samples before: a) and after b) p-irradiation. Spectra are measured using the grating with 600 grooves mm^{-1} .

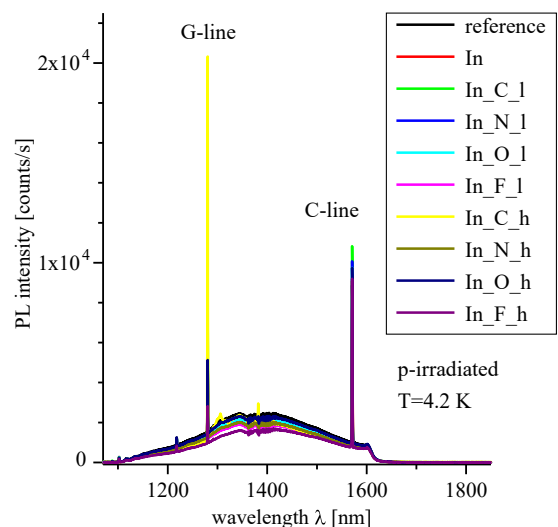


Figure 5. Overview LTPL spectra of the indium implanted samples after p-irradiation. Spectra are measured using the grating with 150 grooves mm^{-1} .

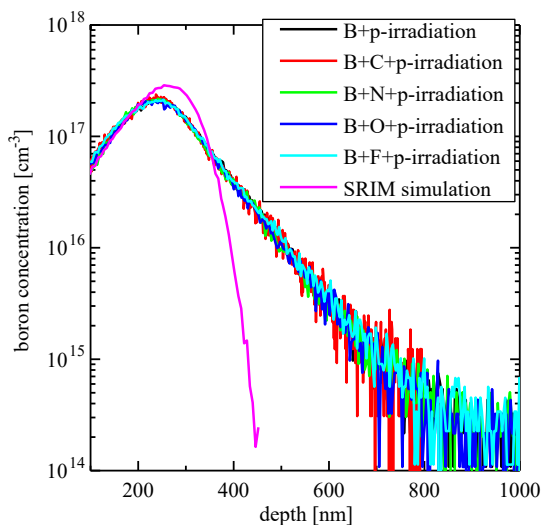


Figure 6. SIMS boron depth profiles of the boron implanted sample with and without a co-implantation after proton irradiation. SIMS profiles are compared to SRIM^[17] simulations of the boron implantation depth profile.

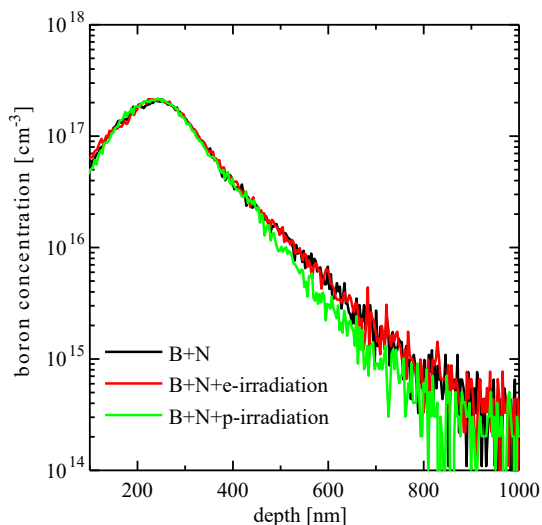


Figure 7. SIMS boron depth profiles of the boron and nitrogen co-implanted samples before and after e- or p-irradiation.

different co-implantations and is, within the experimental error, the same compared to no co-implantation. There is one exception for boron in case of the high dose carbon co-implantation. It can be stated that apart from this exception the co-implantation has no impact on the activation of boron and gallium. The activated fraction of each acceptor in case of the low dose carbon co-implantation was calculated by dividing the measured conductance with the conductance calculated by integrating the concentration from the SIMS depth profiles. In that way, we found an activated fraction of 60%, 65%, and 12% for the boron, gallium, and indium, respectively.

A lower activation of boron was also observed by others in case of high-dose carbon co-implantation.^[9] They discussed possible boron-carbon pairs as reason for the increased deactivation of

boron. But it has to be noted that B_s-C_s pairs are discussed to be acceptors as well.^[10] If this is correct the formation of B_s-C_s pairs should have no impact on the measured sheet resistance. Because the substitution of one acceptor by another acceptor should not change the overall measured sheet resistance.

In case of indium, we find an impact of the co-implantation species on the indium activation after RTP. Since this study is focusing on the effect of the co-implantation species on the acceptor removal phenomenon the individual defect reactions or processes which take place in each case will not be discussed here. Ideas to explain the observed changes in the indium activation can be found elsewhere.^[11]

It should be noted that the small error bars in case of the un-irradiated samples show the applicability and reproducibility of the 4pp measurement method.

From the literature,^[5] it is expected that for the applied proton irradiation an increase in the sheet resistance of one order of magnitude should be seen. If an acceptor removal constant of $c_A = 2 \times 10^{-15} \text{ cm}^2$ is assumed then the active boron concentration should be reduced from $\approx 10^{17} \text{ cm}^{-3}$ to $\approx 10^{16} \text{ cm}^{-3}$, which should induce an order of magnitude increased sheet resistance after proton irradiation. The situation for electron irradiation is different. For the applied electron irradiation conditions, the carrier density should decrease in only negligible amounts.^[12,13]

When the irradiation case is analyzed, a complex picture is found. The error bars are after irradiation much larger making the interpretation difficult. The reason for the larger error bars could not be identified within this work. The measurement setup was ruled out since all samples were measured at the same time under the same conditions. The measurements were repeated also after applying a further HF dip to remove possible charges, which might be introduced into the natural oxide by the irradiation without a change in the signals.

An unexpected reduction of the sheet resistance is found for the case of electron irradiation. This is seen for all boron and gallium samples as well as for most of the indium-implanted samples. The reason for that remains unclear. From the literature, no change in the sheet resistance would be expected and only for higher electron irradiation doses an increase in sheet resistance was found.^[12,13] It seems that additional acceptors are formed by the electron irradiation, which are independent from the implanted acceptor species and hence, would include intrinsic defects such as silicon interstitials and vacancies.

For the proton irradiation, a clear result is found for the gallium- and indium-implanted samples. An increase in the sheet resistance is clearly visible for all investigated samples. This might be due to the larger initial sheet resistance and hence, lower initial doping concentration. Therefore, the effect of acceptor removal is more clearly visible. For gallium, the carbon and oxygen co-implantations have a beneficial effect as expected from literature.^[6,14] In case of indium, an increased sheet resistance for all co-implantation species was found indicating no beneficial effect with respect to the acceptor removal phenomenon.

In case of boron-implantation, the acceptor removal is visible for the sample without co-implantation as well. The sheet resistance increases significantly but the increase is lower than expected from the calculations made before by assuming an acceptor removal constant of $c_A = 2 \times 10^{-15} \text{ cm}^2$.^[5] All B-doped

samples with a co-implanted species, except of high-dose carbon co-implantation, show a lower sheet resistance compared to the sample without co-implantation (blue bars). This indicates a reduced acceptor removal in all samples with a co-implantation. The effect is most pronounced for the low-dose F and high-dose N co-implantation. The sample with a high dose carbon co-implantation is an exception since it has an initially higher sheet resistance. Compared to the initial value the increase of the sheet resistance is smaller than for the sample without co-implantation. This indicates that the acceptor removal is suppressed in this case as well.

The LTPL spectra taken before and after proton irradiation of the samples without a co-implantation are shown in Figure 4. The LTPL peak ratios $B_{NP}(BE)/I_{TA}(FE)$ and $B_{TA}(BE)/I_{TA}(FE)$ for the boron-doped high resistivity reference wafer and the boron implanted sample are compared in Figure 4a; we find a slightly smaller peak ratio for the boron-implanted sample. But for a homogenous distribution of the generated excitons^[15] during laser excitation we should find a two orders of magnitude larger LTPL signal for the boron-implanted sample. This is the case because the integration of the boron atom concentration over the whole wafer thickness leads to a two orders of magnitude higher boron concentration in case of the implantation. Possibly the exciton profile is not homogenous over the sample thickness due to surface recombination of excitons. This could explain why the near surface implantation of boron reveals an even smaller LTPL signal. For the gallium- and indium-implanted samples, the LTPL peaks of acceptor bound excitons $Ga_{NP}(BE)$ and $In_{NP}(BE)$ are clearly seen.

After proton irradiation, the LTPL spectra shown in Figure 4b change significantly. Now the boron- and gallium-related peaks disappeared and a much smaller $In_{NP}(BE)$ peak is seen. Additionally, a so far unknown peak at 1100.8 nm appears. There are two explanations for the disappearance of the acceptor bound excitons. First, the acceptors are deactivated so that the acceptor bound excitons cannot exist anymore. Second, the excitons bind to other defects with a much higher density and hence the probability of an exciton to bind on an acceptor becomes very low. Therefore, LTPL overview spectra were measured. As an example, the indium-implanted samples are shown in Figure 5. Clearly visible are two sharp lines with a high intensity. These lines are found earlier and are called G- and C-line.^[16] Possibly this second explanation is valid and thus, the LTPL spectra cannot be evaluated with respect to the acceptor removal phenomenon.

The LTPL spectra after electron irradiation are even more controlled by the G line. This means that the G line is so intense that the other peaks related to the acceptors are only marginally larger than the noise. Hence, in this case, the LTPL spectra cannot be evaluated with respect to the acceptor removal phenomenon, too.

The boron concentration depth profiles measured by SIMS after proton irradiation for all co-implantation species are shown in Figure 6. Additionally, the SRIM^[17] simulation of the boron implantation depth profile is plotted. The first 100 nm are cut off since they are obscured by SIMS measuring artifacts due to formation of the sputtering equilibrium. The diffusion of boron during the RTP is clearly visible. It is found that the co-implantation species has no impact on the boron diffusion during RTP in

the experiment with a comparable low dose of the boron implantation.

When the SIMS boron profiles before and after different irradiations are compared as done in Figure 7, a small difference is found for the proton irradiation. From 400 to 800 nm, the boron SIMS profile of the proton irradiated sample is significantly below the other two profiles. This is visible for all co-implantation species and also for the samples without a co-implantation. As an example, the boron-implanted sample with nitrogen co-implantation is shown in Figure 7. It should be noted that this shrinking cannot be responsible for the increase in sheet resistance since it is too small to explain that observed increase.

The reason for this shrinking of the boron depth profile by proton irradiation is puzzling. If we assume the boron is mobile during irradiation then a broadening of the boron profile due to the concentration gradient should be observed. This is clearly not seen. Can it be possible that a nuclear reaction in a way that the boron reacts to, e.g., beryllium takes place during proton bombardment? In that case, the loss in boron should be proportional to the initial boron concentration and hence, be also visible for the highest boron concentration, which is also not seen. Since no broadening of the boron profile is visible, one can state that a process involving diffusion of boron seems to be unlikely.

For the gallium- and indium-implanted samples, the SIMS concentration profiles were taken before and after proton and electron irradiation as well. No changes in the profiles due to the irradiation could be found.

One explanation approach for the acceptor removal phenomenon is the boron pairing reaction with oxygen forming the B_i-O_i -defect.^[5,18] Therefore, it is necessary for the boron to be mobile at room temperature which is a debatable idea.^[19,20] Assuming an interstitial oxygen concentration in FZ silicon used for LGADs of about 10^{15} cm^{-3} then the distance for the boron to reach an interstitial oxygen atom is about 50 nm. A diffusion of boron for such a long distance at room temperature would be clearly visible in our SIMS data. Since this is not seen this explanation approach seems to be unlikely.

Another explanation which is not based on the fast diffusion of boron at room temperature is the $B_{Si}-Si_i$ -defect^[21] approach. In that case the negatively charged substitutional boron captures a positively charged silicon interstitial atom which is released during irradiation. The $B_{Si}-Si_i$ -defect is in its ground state a positively charged donor, which can be transformed in the activated configuration due to the injected carriers during irradiation. In the latter configuration it is a neutral defect.^[22] After this defect reaction, the acceptor substitutional boron is not available for the gain layer any more.

5. Summary and Conclusion

LGAD with a gain of about 10 are very fast $n^{++}-p^+-p^--p^{++}$ -detectors with comparatively low noise. There is one disadvantage which is related to the radiation hardness of the LGADs. Under irradiation, the gain is lost due to an acceptor removal phenomenon, which deactivates the acceptors and causes a decrease in the doping concentration of the p^+ -layer.

In this contribution, this acceptor removal phenomenon was investigated. The experiment focused on the three acceptors boron, gallium, and indium. These acceptors were implanted into high resistivity silicon. Additionally, four co-implantation species (oxygen, nitrogen, carbon, and fluorine) were implanted as well. After RTP annealing to activate the acceptors, the samples were irradiated by electrons and protons. To investigate the acceptor removal phenomenon three measurement methods were applied before and after irradiation. These were 4pp) measurement, LTPL, and SIMS. The first two measurements reveal the electrical active acceptors and the latter one reveals the total boron atom concentration as a function of depth. In the sheet resistance measurements for the proton irradiated samples, the acceptor removal for all investigated acceptors was observed whereas for the electron irradiation an unexpected decrease in the sheet resistance was found. As a result, for the proton irradiation, it was found that in case of boron acceptors the low-dose fluorine co-implantation and the high-dose nitrogen co-implantation have the most beneficial effect on the acceptor removal phenomenon. For gallium, the low-dose carbon and low-dose oxygen co-implantation are beneficial and in the case of indium all co-implantation species amplify the effect of acceptor removal. The LTPL measurements show a disappearance of the acceptor-related PL peaks after proton irradiation, too. This can be related to an acceptor removal after proton irradiation. But it could be also possible that the excitons move to other defects which are generated by the irradiation. Indeed two very intensive PL peaks called G- and C-line are found in the irradiated samples making the latter explanation more likely. The SIMS measurements of the boron concentration depth profiles do not show any change due to the type of co-implantation. Also, the gallium- and indium-implanted samples do not show any change in the SIMS concentration profiles before and after electron and proton irradiation. The same was observed in the boron case for the unirradiated and electron-irradiated samples. In the proton irradiation case, a puzzling shrinking or decrease in the boron concentration from 400 to 800 nm is observed. Diffusion of boron is unlikely since it would be a movement against the boron concentration gradient. Also, a nuclear reaction seems to be unlikely since this would be proportional to the boron concentration and such proportionality is not found. This observed shrinking remains an unresolved question.

Two explanation approaches for the acceptor removal phenomenon are discussed, namely the formation of a B_i-O_i -defect and the formation of a $B_{Si}-Si_i$ defect. The first one relies on a fast movement of boron at room temperature. This could not be confirmed under the applied conditions by our SIMS measurements, and hence this explanation approach seems to be unlikely. The second one, where a substitutional boron atom captures a silicon interstitial atom and forms a $B_{Si}-Si_i$ defect seems to be more likely since it does not involve an unlikely fast boron diffusion at room temperature.

Acknowledgements

Dirk Schulze (TU Ilmenau, Institute of Physics) is greatly acknowledged for LTPL measurements. This work was supported by the project DELGAD of the BMWi (49MF190042).

Open Access funding enabled and organized by Projekt DEAL.

Conflict of Interest

The authors declare no conflict of interest.

Data Availability Statement

The data that support the findings of this study are available from the corresponding author upon reasonable request.

Keywords

acceptor removal, low-gain avalanche detector (LGAD), silicon

Received: March 15, 2022

Revised: May 16, 2022

Published online: June 19, 2022

- [1] H. F.-W. Sadrozinski, A. Seiden, N. Cartiglia, *Rep. Prog. Phys.* **2017**, *81*, 026101.
- [2] G. Paternoster, R. Arcidiacono, M. Boscardin, N. Cartiglia, F. Cenna, G. F. D. Betta, M. Ferrero, R. Mulargia, M. Obertino, L. Pancheri, C. Piemonte, V. Sola, *J. Instrum.* **2017**, *12*, C02077.
- [3] G. Pellegrini, M. Baselga, M. Carulla, V. Fadeyev, P. Fernández-Martínez, M. F. García, D. Flores, Z. Galloway, C. Gallrapp, S. Hidalgo, Z. Liang, A. Merlos, M. Moll, D. Quirion, H. Sadrozinski, M. Stricker, I. Vila, *Nucl. Instrum. Methods Phys. Res., Sect. A* **2016**, *831*, 24.
- [4] M. Ferrero, R. Arcidiacono, M. Barozzi, M. Boscardin, N. Cartiglia, G. F. D. Betta, Z. Galloway, M. Mandurrino, S. Mazza, G. Paternoster, F. Ficorella, L. Pancheri, H.-F. W. Sadrozinski, F. Siviero, V. Sola, A. Staiano, A. Seiden, M. Tornago, Y. Zhao, *Nucl. Instrum. Methods Phys. Res., Sect. A* **2019**, *919*, 16.
- [5] M. Moll, in *Proc. 28th Int. Workshop On Vertex Detectors — PoS(Vertex2019)*, Sissa Medialab, Lopus, Croatia, **2020**, p. 027.
- [6] R. Padilla, C. Labitan, Z. Galloway, C. Gee, S. M. Mazza, F. McKinney-Martinez, H. F.-W. Sadrozinski, A. Seiden, B. Schumm, M. Wilder, Y. Zhao, H. Ren, Y. Jin, M. Lockerby, V. Cindro, G. Kramberger, I. Mandiz, M. Mikuz, M. Zavrtnik, R. Arcidiacono, N. Cartiglia, M. Ferrero, M. Mandurrino, V. Sola, A. Staiano, *J. Inst.* **2020**, *15*, P10003.
- [7] G. Kramberger, M. Baselga, V. Cindro, P. Fernandez-Martinez, D. Flores, Z. Galloway, A. Gorišek, V. Greco, S. Hidalgo, V. Fadeyev, I. Mandić, M. Mikuz, D. Quirion, G. Pellegrini, H. F.-W. Sadrozinski, A. Studen, M. Zavrtnik, *J. Inst.* **2015**, *10*, P07006.
- [8] D. K. Schroder, *Semiconductor Material and Device Characterization*, 3rd ed., Wiley-IEEE Press, Piscataway, NJ; Hoboken, NJ **2006**.
- [9] H.-C. Liao, J.-C. Lin, R.-D. Chang, *Jpn. J. Appl. Phys.* **2018**, *57*, 081301.
- [10] C. E. Jones, D. Schafer, W. Scott, R. J. Hager, *J. Appl. Phys.* **1981**, *52*, 5148.
- [11] P. Pichler, *Intrinsic Point Defects, Impurities, and their Diffusion in Silicon*, Springer, Wien **2004**.
- [12] A. R. Bean, S. R. Morrison, R. C. Newman, R. S. Smith, *J. Phys. C: Solid State Phys.* **1972**, *5*, 379.
- [13] S. J. Taylor, M. Yamaguchi, S. Matsuda, T. Hisamatsu, O. Kawasaki, *J. Appl. Phys.* **1997**, *82*, 3239.
- [14] G. Lindström, M. Ahmed, S. Albergo, P. Allport, D. Anderson, L. Andricek, M. M. Angarano, V. Augelli, N. Bacchetta, P. Bartalini, R. Bates, U. Biggeri, G. M. Bilei, D. Bisello, D. Boemi, E. Borch, T. Botila, T. J. Brodbeck, M. Bruzzi, T. Budzynski, P. Burger, F. Campabadal, G. Casse, E. Catacchini, A. Chilingarov, P. Ciampolini, V. Cindro, M. J. Costa, D. Creanza, P. Clauws, et al., *Nucl. Instrum. Methods Phys. Res., Sect. A* **2001**, *466*, 308.
- [15] M. A. Tamor, J. P. Wolfe, *Phys. Rev. Lett.* **1980**, *44*, 1703.

- [16] G. Davies, S. Hayama, L. Murin, R. Krause-Rehberg, V. Bondarenko, A. Sengupta, C. Davia, A. Karpenko, *Phys. Rev. B* **2006**, *73*, 165202.
- [17] J. F. Ziegler, M. D. Ziegler, J. P. Biersack, *Nucl. Instrum. Methods Phys. Res., Sect. B* **2010**, *268*, 1818.
- [18] C. Liao, E. Fretwurst, E. Garutti, J. Schwandt, M. Moll, A. Himmerlich, Y. Gurimskaya, I. Pintilie, A. Nutescu, Z. Li, L. Makarenko, *IEEE Trans. Nucl. Sci.* **2022**, *69*, 576.
- [19] L. Vines, E. V. Monakhov, A. Y. Kuznetsov, R. Kozłowski, P. Kaminski, B. G. Svensson, *Phys. Rev. B* **2008**, *78*, 085205.
- [20] R. D. Harris, G. D. Watkins, L. C. Kimerling, *Mater. Sci. Forum* **1986**, *10–12*, 163.
- [21] C. Möller, K. Lauer, *Phys. Status Solidi RRL* **2013**, *7*, 461.
- [22] K. Lauer, C. Möller, C. Tessmann, D. Schulze, N. V. Abrosimov, *Phys. Status Solidi C* **2017**, *14*, 1600033.